Reflection of TE_{0n} Modes at Open-Ended Oversized Circular Waveguide

Manfred Thumm, *Fellow, IEEE*, Walter Kasparek, Dietmar Wagner, *Member, IEEE*, and Andreas Wien

***Abstract*—Reflection of circular symmetric TE_{0n} modes (n = 1–6) at an oversized, open-ended circular waveguide (C76-waveguide, inner diameter = 27.79 mm, 70 GHz) radiating into free space has been investigated theoretically employing two scattering matrix codes (SMCs), the finite-difference time-domain code EMPIRE and the uniform geometrical theory of diffraction (UTD) as well as the first time experimentally. The measurements utilized mode converters for generation of pure TE_{0n} modes and a wavenumber spectrometer for mode analysis in the oversized waveguide. The total power reflection computed by EMPIRE is 4.1 to 13.4 dB lower than calculated from free-space wave and waveguide mode impedances. In all cases, most of the reflected power is carried by the backward traveling TE_{01} mode, which is the mode closest to cutoff. Experiments are in very good agreement with theoretical results.**

***Index Terms*—Circular symmetric TE_{0n} modes, FDTD, gyrotrons, mode matching, open-ended waveguide, reflection, UTD.**

I. Introduction

REFLECTION in standard rectangular and circular waveguides always is in the same fundamental mode. There is no mode conversion to higher order modes like in oversized waveguides. The objective of the present work is a systematic theoretical and experimental study to show the peculiarities of reflection in overmoded waveguides, here for the example of the mode series TE_{0n} with n = 1–6 at the frequency of 70 GHz in the C76-circular waveguide (inner diameter I.D. = 27.79 mm). These modes show relatively low ohmic attenuation and therefore have been employed as interaction and output modes of 100-kW-class gyrotron oscillators and amplifiers [1]. Such gyrotron oscillators in the frequency range from 28 GHz (TE_{01} mode) to 384 GHz (TE_{08} mode) are utilized for fusion plasma diagnostics, materials processing, and various types of millimeter wave and subterahertz spectroscopy. Ka-band and W-band gyro-amplifiers are applied in high-power RADAR systems. Reflection at the circular waveguide output of higher than approximately −15 dB could strongly reduce the electronic efficiency in the interaction circuits of these gyro-devices. In order to facilitate experimental studies, the present measurements have been conducted at low power (50 mW).

TABLE I
Coupling Constants $K^{\pm}_{m1}$ for Forward- and Backward-Wave Coupling of an Incident TE_{01} Mode at an Abrupt Waveguide Radius Step ($k_0 a$ = 20.39)

Coupled mode	TE_{02}	TE_{03}	TE_{04}	TE_{05}	TE_{06}
Forward coupling	1.557	0.880	0.632	0.508	0.492
Backward coupling	-0.035	-0.055	-0.082	-0.127	-0.278

In circular overmoded waveguides the coupling coefficient for conversion of TE_{0n} to TE_{0m} modes at a small abrupt step Δa of the waveguide radius a is given by [2]

$$C^{\pm}_{mn} = \frac{X'_{0m} X'_{0n}}{X'^2_{0m} - X'^2_{0n}} \frac{\beta_{0m} \pm \beta_{0n}}{\sqrt{\beta_{0m}\beta_{0n}}} \times \frac{\Delta a}{a} \quad (1)$$

$$= K^{\pm}_{mn} \times \frac{\Delta a}{a} \quad (2)$$

where $\beta_{0n} = k_0\sqrt{1 - (X'_{0n}/k_0 a)^2}$ is the axial wavenumber (phase constant) with $k_0 = 2\pi/\lambda_0$ being the free-space wavenumber and X'_{0n} the zero of the corresponding Bessel function derivative. The ± signs are for coupling to forward and backward traveling waves, respectively. For an inner diameter (I.D.) = 27.79 mm at 70 GHz ($k_0 a$ = 20.39), the coupling constants $K^{\pm}_{m1}$ in (2) for an incident TE_{01} wave are summarized in Table I.

The strongest coupling in forward direction is to the nearby TE_{02} mode, whereas the major coupling in backward direction is to TE_{08}, which is the mode closest to cutoff (X'_{0n} = 19.616). There is no coupling to the cross-polarized TM_{0n} modes [2].

In highly oversized circular waveguides, the transmission of a waveguide mode through a large, abrupt step in radius asymptotically corresponds to the radiation from an open-ended waveguide (semi-infinite circular waveguide). It has been demonstrated in Wien and Thumm [3] and Wagner *et al.* [4] that mode-matching methods based on the generalized scattering matrix can be used for verification. Theoretical results for the reflection of 70-GHz TE_{0n} modes (n = 1–6) at an open-ended C76-waveguide employing these two scattering matrix codes (SMCs) [3], [4] and a commercial finite-difference time-domain code (FDTD EMPIRE) [5] are summarized in Section II.

Backscattering of waveguide modes due to abrupt changes of the geometry is caused by edge diffraction leading to an additional field to the incident and reflected waves. This diffracted field can be interpreted as anisotropic radiation from a line source located at the edge, which can be described by equivalent currents. In Yee *et al.* [6], a ray optical approach was developed to estimate reflections from open-ended semi-infinite circular waveguides. This method can be applied if the incident rays are perpendicular to the edge and the diffracted rays that contribute to the reflected power are lying on Keller's diffraction cone (GTD, [7]) which is the case for reflection of $\mathbf{TE}_{0n}$ modes. In this scalar problem, there is only coupling between these circular symmetric modes $(\Delta m = 0)$, no change in azimuthal mode index, and no coupling to TM modes. However, Yee *et al.* [6] assume the approximation of low-order modes $\cos\theta_{nm} = \beta_{nm}/k_0 \approx 1$ where they could compare with the exact theory of Weinstein [8]. This method takes care for multiple diffractions and arbitrary flange angles but leads to asymmetric results $S_{nq} \neq S_{qn}$, as will be shown in Section II. Wien and Thumm [9] employed the method of equivalent edge currents (MECs) [10] and derived formulas that are also valid for high-order modes. For circular symmetric modes $(m = 0)$, the reflection due to primary diffraction can be written as

$$S_{nq} = \frac{j}{\pi k_0^2 a^2 J_0\left(X'_{0n}\right) J_0\left(X'_{0q}\right)} \times \frac{\sqrt{1-\cos\theta_{0n}}\sqrt{1-\cos\theta_{0q}}}{\sqrt{\cos\theta_{0n}\cos\theta_{0q}}\sqrt{\sin\theta_{0n}\sin\theta_{0q}}\left(\cos\theta_{0n}+\cos\theta_{0q}\right)}. \quad (3)$$

Results using this improved theory are also given in Section II. Section III introduces the measurement techniques used for experimental verification. In Section IV, the measurements utilizing a wavenumber spectrometer are compared with the theoretical results, and the conclusions are drawn in Section V.

II. Theoretical Results

Reflection of circular symmetric $\mathbf{TE}_{0n}$ modes ($n = 1$–6) at 70 GHz from an oversized, open-ended circular C76-waveguide (I.D. = 27.79 mm) radiating into free space has been investigated theoretically employing two SMCs [3], [4], a commercial finite-difference time-domain code (FDTD EMPIRE) [5] and the MEC [9], [10], the uniform geometrical theory of diffraction (UTD).

In the case of the SMC calculations, the diameter of the highly oversized output waveguide and the number of considered modes were stepwise increased to get asymptotic results approximately corresponding to radiation into the free space from a flanged waveguide end [see Fig. 1(right)]. The results from the two SMCs were in excellent agreement. Table II summarizes for the incident modes $\mathbf{TE}_{0n}$ ($n = 1$–6) the reflection in the different modes, the total reflection (uncertainty ±2 dB), and the reflection calculated from the free-space wave impedance $Z_0 = \sqrt{\mu_0/\varepsilon_0} = 376.63\ \Omega$, and the waveguide mode impedances $Z_{0n} = (k_0/\beta_{0n})Z_0$. In all cases, most of the reflected power is carried by the backward traveling $\mathbf{TE}_{08}$ mode, which is the mode closest to cutoff. Power reflection calculated from the SMCs is 7.3 to 15.6 dB lower than calculated from free-space wave and waveguide mode impedances.

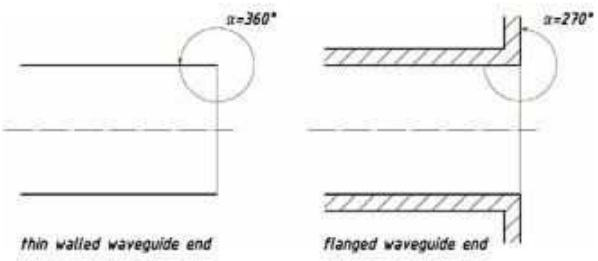

Fig. 1. Waveguide end geometries for UTD computations.

TABLE II
Reflection in $\mathbf{TE}_{0n}$ Modes ($n = 1$–6) Calculated With Scattering Matrix and FDTD Codes for Different Incident Modes. The Total Reflection is Compared With the Reflection Calculated From Free-Space Wave and Waveguide Mode Impedances

Reflection [dB]: Scattering Matrix Code/FDTD EMPIRE™							
		Incident Mode					
		TE_{01}	TE_{02}	TE_{03}	TE_{04}	TE_{05}	TE_{06}
Reflected Mode	TE_{01}	-77/-70	-72/-66	-66/-62	-63/-58	-57/-54	-48/-46
	TE_{02}	-72/-66	-67/-60	-62/-56	-58/-53	-52/-48	-42/-40
	TE_{03}	-67/-62	-62/-56	-57/-52	-53/-49	-48/-44	-38/-35
	TE_{04}	-63/-58	-57/-53	-53/-49	-48/-46	-42/-40	-34/-31
	TE_{05}	-60/-54	-52/-48	-48/-44	-43/-40	-38/-35	-28/-26
	TE_{06}	-50/-46	-42/-40	-38/-36	-33/-31	-28/-26	-17/-16
	Total	-48.2/ -45.0	-41.4/ -39.0	-37.4/ -35.0	-32.4/ -30.3	-27.4/ -25.2	-16.6/ -15.4
	$\frac{Z_0 - Z_{0n}}{Z_0 + Z_{0n}}$	-40.9	-30.0	-22.9	-17.2	-11.8	-4.9

In case of the FDTD simulations, a circular waveguide port with a diameter of 27.79 mm and a wall thickness of 1.65 mm (C76-waveguide) has been created in a free-space environment, which has a total size of 60 mm × 60 mm × 80 mm (Fig. 2). In order to simulate up to 80 GHz, a cell spacing of 0.25 mm has been used yielding to about 20 million cells. Absorbing boundary conditions (PMLs) have been applied at the simulation boundaries. Waveguide modes are precalculated by the code in ascending order of their cutoff frequency and used for excitation and decomposition at the port. Up to 200 modes have been calculated including the modes of interest $\mathbf{TE}_{01}$ to $\mathbf{TE}_{08}$. For each incident mode, a separate simulation has to be carried out that yields one column of the scattering matrix. On a dual Intel Xeon E2690 PC, one simulation needed about 2 hours with a memory requirement of 5 GB. In comparison to this, the SMC and UTD calculation times are only 10 min and 1 s, respectively.

Power reflection calculated from FDTD EMPIRE is 4.1 to 13.4 dB lower than calculated from free-space wave and waveguide mode impedances (Table II). The SMC calculations result in a somewhat lower total reflection compared with the

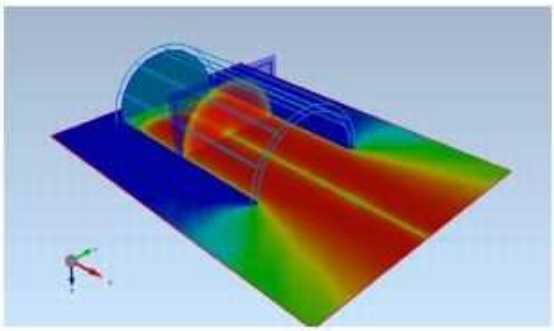

Fig. 2. Waveguide end geometry and electric field of the open-ended oversized waveguide excited by the TE_{01} mode (FDTD computations).

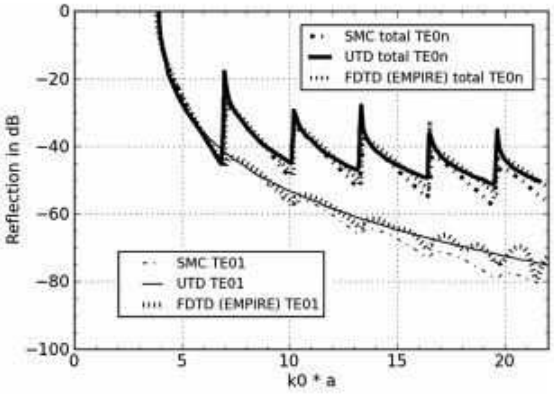

Fig. 3. Reflection calculated using the SMC, UTD (formula (3)) and FDTD methods in dependence of the normalized waveguide radius k_0a for the incident TE_{01} mode. Upper curves (upper legend): total reflection. Lower curves (lower legend): reflection into the incident TE_{01} mode.

FDTD simulations. The reason for this probably is that the SMC method employs a step to a very large but nevertheless finite waveguide radius and not radiation into free space.

UTD calculations have been performed for the cases thin-walled waveguide ($\alpha = 360°$) and flanged waveguide ends ($\alpha = 270°$), as shown in Fig. 1.

The curves in Fig. 3 show reflection versus normalized waveguide radius k_0a for the incident TE_{01} mode calculated by the SMC, UTD, and FDTD methods. In the case of UTD a thin-walled waveguide was used. The upper curves (upper legend) give the total reflection in all propagating TE_{0n} modes ($n = 1$–6) and the lower curves (lower legend) the back reflection into the TE_{01} mode. For very low reflection (lower than approximately −70-dB) numerical uncertainties of the FDTD simulations show up. UTD formula (3) [9] leads like the SMC and FDTD methods to symmetric results: $S_{nq} = S_{qn}$.

The main part of the reflected power is carried away by the modes which are closest to cutoff. The corresponding k_0a values are the zeros of the Bessel function derivative for the modes TE_{02} to TE_{06}. For the higher TE_{0n} modes ($n = 2$–6) at $k_0a = 20.39$ (I.D. = 27.79 mm, 70 GHz), the results of the reflection are given in Tables II and III.

TABLE III
REFLECTION IN THE MAIN MODES CALCULATED BY THE SMC, FDTD, AND UTD METHODS FOR INCIDENT TE_{0n} MODES WITH $n = 2$–6. THE ANGLES $\alpha = 360°$ AND 270° CORRESPOND TO THIN-WALLED AND FLANGED OPEN-ENDED WAVEGUIDE, RESPECTIVELY

		Reflection [dB]			
Incident Mode	Reflected Mode	SMC/FDTD Codes	UTD [6] $\alpha = 360°$	UTD [6] $\alpha = 270°$	UTD [9] $\alpha = 360°$
TE_{02}	TE_{06}	-43 / -40	-43.1	-43.7	-41.3
TE_{03}	TE_{06}	-38 / -36	-36.0	36.5	-37.1
TE_{04}	TE_{06}	-33 / -31	-30.1	-30.5	-33.0
TE_{05}	TE_{06}	-28 / -26	-24.3	-24.7	-28.1
	TE_{05}	-38 / -35	-35.5	-36.0	-36.7
	TE_{04}	-42 / -40	-39.3	-39.9	-41.2
TE_{06}	TE_{06}	-18 / -16	-15.6	-15.9	-18.1
	TE_{05}	-28 / -26	-28.0	-28.4	-28.1

III. Experimental Arrangements

A. Generation of the TE_{01} Mode

Low-power millimeter waves were generated by a CW Gun oscillator (70 GHz, 50 mW) in fundamental rectangular waveguide (*V*-band). A pure TE_{01} mode was produced by a geometrical Marié TE_{10} (rectangular)-to-TE_{01} (circular) mode transducer followed by long sections of helix-waveguide mode filters and an optimized nonlinear TE_{01}-mode up-taper from the small diameter circular waveguide (I.D. = 8 mm) to the highly oversized circular waveguide (I.D. = 27.79 mm).

B. Generation of TE_{0n} Modes With $n = 2$–6

Oversized mode transducers with small circular symmetric, periodic diameter perturbations ("rippled-wall") convert TE_{0n}-mode into $TE_{0,n+1}$-mode power provided that the waveguide diameter is periodic approximately with the beat wavelength λ_B $(n, n+1)$ of the two modes [11]. Unwanted power conversion to other coupled modes is minimized by numerically solving the corresponding coupled-wave differential equations. The optimum wavelength λ_W $(n, n+1)$ of the wall perturbations differs slightly from λ_B $(n, n+1)$. The efficiencies are further improved by superimposing small amounts of additional, phase matched, higher harmonics on the wall structure and/or by inserting cylindrical phase shifters. The TE_{0n} modes with $n = 2$–6 can be generated from the TE_{01} mode by cascading the corresponding single-step mode transducers. The calculated conversion efficiencies range from 99.7% for the TE_{01}-to-TE_{02} mode converter to 98.2% for the TE_{05}-to-TE_{06} converter, with an overall TE_{01}-to-TE_{06} conversion efficiency of 94.6% (ohmic attenuation is included) [12]. The mode converter sequence has been manufactured by direct machining on a numerically controlled lathe and assembled from individual sections (aluminium waveguide with input and output diameters of 27.79 mm).

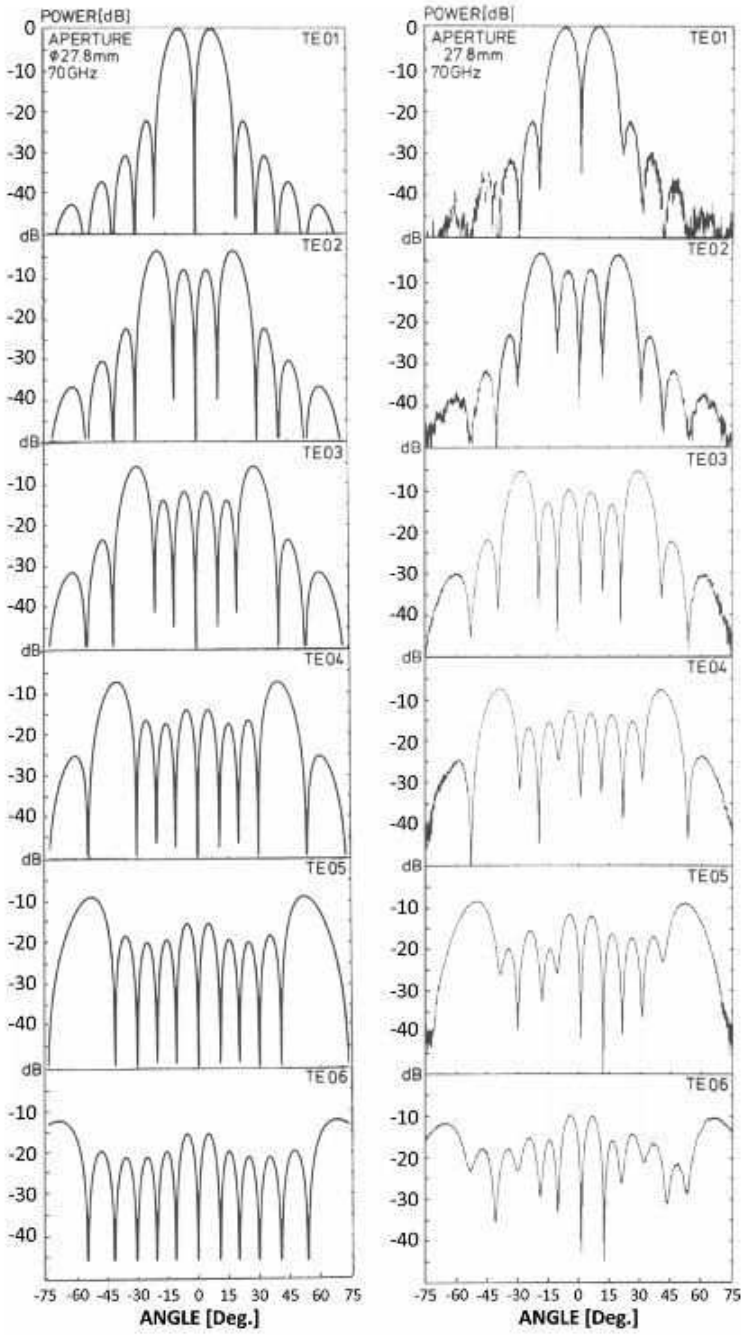

Fig. 4. Computed (left) and measured (right) far-field patterns of TE_{0n} modes (n = 1–6) successively generated by rippled-wall mode converters (f = 70 GHz, a_n = 13.9 mm, 5 dB/div. vertical and 15 deg./div. horizontal).

In Fig. 4 the measured far-field radiation patterns of the TE_{0n} modes (n = 2–6) successively produced from a pure TE_{01} input mode (also shown) are plotted together with the calculated mode patterns. The agreement of these far-field patterns is very good and consistent with the calculated conversion efficiencies and experimental efficiencies deduced from measurements employing a wavenumber spectrometer [12].

C. Wavenumber Spectrometer (k-Spectrometer)

In order to measure the spectrum of forward- and backward-traveling waves in highly oversized waveguides, the "k-spectrometer" developed by Kasparek and Müller [13] was used. In this instrument, the free-space radiation of a leaky-wave antenna (axial array of equidistant holes) in the waveguide wall is used

Fig. 5. Photograph of the wavenumber spectrometer showing the circular waveguide with the 1.2-m-long hole array and two receiver antennas, one being controlled by a motor drive.

TABLE IV
WAVENUMBER SPECTROMETER ELEVATION ANGLES OF FORWARD- AND BACKWARD-PROPAGATING TE_{0n} MODES ($n = 1$–6) FOR I.D. = 27.79 mm AT 70 GHz

Mode	Elevation Angle θ (deg.)	
	Forward	Backward
TE_{01}	10.8	169.2
TE_{02}	20.1	159.9
TE_{03}	29.9	150.1
TE_{04}	40.8	139.2
TE_{05}	53.9	126.1
TE_{06}	74.1	105.9

for mode analysis. The radiation pattern of this array depends on the phasing of each radiating hole, which is given by the axial wave number of the exciting waveguide mode. The main lobe of this pattern has an elevation angle θ with respect to the axial direction of the waveguide, which is given by $\cos\theta = \beta_{0n}/k_0$. The polarization of the detected field allows to distinguish TE from TM modes. TE_{0n} modes only can be seen in the $\vec{E} \perp \vec{k}$ spectrum.

The k-spectrometer shown in Fig. 5 consists of a 2-m-long waveguide, in which the array of 600 holes is milled [13].

The hole diameter varies from 1.0 mm (center) to 0.6 mm (edge), such that a Gaussian taper is formed. This allows to detect the elevation angle θ of the main lobe in the near field of the hole array by pivoting a receiver antenna with high directivity. This antenna is a prime focus parabolic reflector antenna with a rectangular feed horn, which offers an angular resolution (FWHM) of 2° with a suppression of the cross-polarization of 33 dB. The received signal is detected by a fundamental mixer and a spectrum analyzer. The receiver antenna is mounted at an arm, which can be swept around the center of the array by means of a precise motor drive with an angle encoder. To avoid stray radiation, the system is shielded by two microwave absorbing plates.

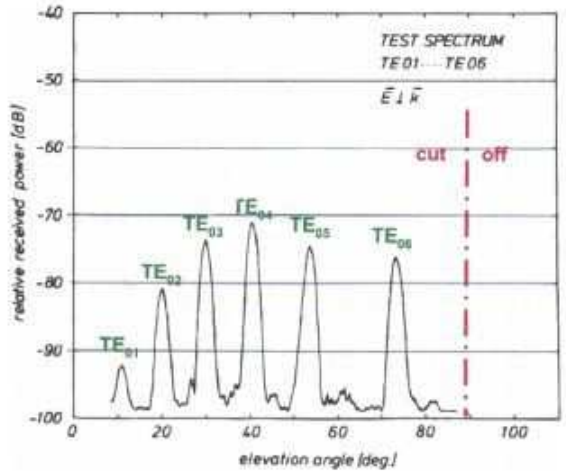

Fig. 6. Spectrum of the TE_{0n} mode mixture (4.6% TE_{01}, 19.1% TE_{02}, 31.4% TE_{03}, 28.3% TE_{04}, 14.2% TE_{05}, and 2.4% TE_{06}) used for calibration.

The elevation angles of forward- and backward-travelling TE_{0n} modes ($n = 1$–6) are summarized in Table IV.

D. Calibration of the k-Spectrometer

The calibration of the k-spectrometer can be done either by a calculation or experimentally by measuring the patterns of different modes with known mm-wave power [13]. The calculation including the wall field, the coupling damping of the holes, and the radiation pattern for each mode can only deliver relative values, as many mechanical parameters are not known exactly due to mechanical tolerances. Experimentally, a straightforward calibration can be done by measuring the spectra of the pure modes generated by the rippled-wall mode converters (see Section III-B). A more simple solution is the excitation of a whole spectrum of modes from a single mode by an abrupt step in the waveguide diameter. This is shown in Fig. 6, where the TE_{01} mode in an 8-mm-diameter waveguide excites a TE_{0n} spectrum ($n = 1$–6, fractions obtained from an SMC are given in the caption of Fig. 6) at the diameter step 8 mm → 27.79 mm, which can be used for calibration.

Table V compares calculated calibration values with weighted data from spectra of pure modes and the test spectrum shown in Fig. 6. One can see that, in spite of many approximations (e.g., the radial electric fields are neglected, the receiver antenna is treated as one-dimensional) and uncertainties (linearity of the detection system, mechanical tolerances, adjustment of the receiver antenna), a good agreement is found.

TABLE V
RELATIVE CALCULATED AND MEASURED COUPLING FACTORS FOR TE_{0n} MODES AT 70 GHz, I.D. = 27.79 mm

Mode	Coupling Factors [dB] Calculated	Measured
TE_{01}	0.0	1.3
TE_{02}	6.6	6.8
TE_{03}	10.2	11.7
TE_{04}	13.3	14.5
TE_{05}	15.3	14.7
TE_{06}	21.2	20.6

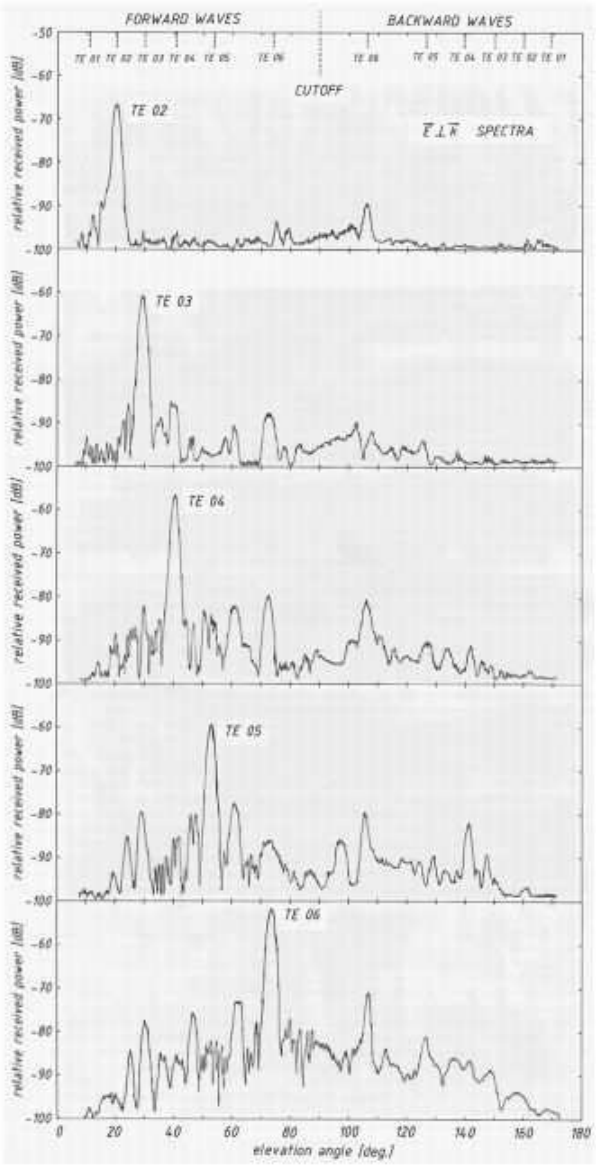

Fig. 7. Wavenumber spectra measured for incident TE_{0n} modes ($n = 2$–6) radiated from an open-ended waveguide at $f = 70$ GHz and I.D. = 27.79 mm.

TABLE VI
COMPARISON OF REFLECTION MEASURED IN THE MAIN MODES WITH THE RESULTS OF SMC, FDTD, AND UTD CALCULATIONS (SEE TABLE III)

Incident Mode	Reflected Mode	Reflection [dB] Measure-ment	SMC FDTD Codes		UTD [6] $\alpha = 360°$	UTD [9] $\alpha = 360°$
TE_{02}	TE_{06}	-40±4	-43	-40	-43.1	-41.3
TE_{03}	TE_{06}	-38±4	-38	-36	-36.0	-37.1
TE_{04}	TE_{06}	-31±2	-33	-31	-30.1	-33.0
TE_{05}	TE_{06}	-26±2	-28	-26	-24.3	-28.1
	TE_{05}	-34±4	-38	-35	-35.5	-36.7
	TE_{04}	-36±4	-42	-40	-39.3	-41.2
TE_{06}	TE_{06}	-18±2	-18	-16	-15.6	-18.1
	TE_{05}	-27±4	-28	-26	-28.0	-28.1

IV. EXPERIMENTAL RESULTS

Measurements were performed employing the experimental arrangements and calibration techniques described in Section III. The open-ended oversized circular waveguide (I.D. = 27.79 mm, C76-waveguide) had a wall thickness of 1.65 mm $\approx 0.4\lambda_0$ and radiated into an anechoic chamber. Since for the lowest order TE_{01} mode, the reflected power in the backward-travelling TE_{06} mode is only -50 dB, no measured signal could be observed (in the noise floor). The $\vec{E} \perp \vec{k}$ wavenumber spectra generated by the incident TE_{0n} modes ($n = 2$–6) are plotted in Fig. 7. The experimental results with down to -40-dB reflection (close to noise level) are summarized in Table VI together with the theoretical values of Table III. The agreement between measurements and theoretical results is very good. Especially, the difference between the measured data and the reflection calculated from the impedance formula (last line in Table II) is huge and clearly rules out the use of this formula for oversized waveguide problems.

V. CONCLUSION

Circular symmetric TE_{0n} modes have relatively low ohmic losses. For that reason, they have been utilized as operating and output modes of 100 kW-class gyro-devices. The present paper reports on first measurements of reflection of 70 GHz TE_{0n} modes ($n = 1$–6) at an open-ended circular C76-waveguide employing mode converters for generation of pure TE_{0n} modes and a wavenumber spectrometer for analysis of the spectra of reflected modes in the oversized waveguide ($k_0 a = 20.39$). The experiments are in very good agreement with theoretical results from FDTD EMPIRE and UTD calculations. The SMC calculations result in a somewhat lower total reflection compared with the FDTD simulations. The reason for this probably is that the SMC method employs a step to a very large, but nevertheless finite, waveguide radius and not radiation into free space.

Power reflection at highly oversized open-ended waveguides is much lower than calculated from the simple reflection coefficient formula using free space wave and waveguide mode

impedances. In the present example of TE_{0n} modes ($n = 1$–6) in C76-waveguide at 70 GHz, the difference is 4.1 to 13.4 dB. Since for the TE_{06} mode at 70 GHz, the ratio of the C76-waveguide radius to the cutoff radius only is 1.04, for all six TE_{0n} modes most of the reflected power is propagating in the backward-traveling TE_{06} mode. The incident TE_{06} mode shows the highest reflection coefficient of approximately -16 dB. Because usually the radius ratio of gyrotron output waveguide and cavity is much larger than 1.04, even for a TE_{06} mode, gyrotron reflection at the open-ended output waveguide is sufficiently low and will not influence the interaction efficiency.

The reason for the observed reflection behavior is that at the transition of the cylindrical waveguide with $k_{0,6} = 20.39$ to an open half-sphere (free space), there is already in the last part of the waveguide a tapered matching of the waveguide mode impedance to the free-space wave impedance. Piefke [14] and others [15], [16] modeled this transition of the circular waveguide ending with a plane screen (flanged waveguide) to free space by a so-called 3-dimensional intermediate medium. Since this intermediate region is a sphere with a radius equal to the waveguide radius, which is for highly oversized waveguides large compared with the wavelength, this transition region is long and provides a good taper leading to low reflection. Since the backscattering of waveguide modes due to abrupt changes of the geometry is caused by edge diffraction, the main part of the reflected power is carried by the backward-traveling mode which is closest cutoff (here the TE_{06} mode). This mode has the highest electrical field close to the waveguide wall and is most strongly excited. In the present example of TE_{0n} modes, there is no coupling to backward-traveling cross-polarized TM_{0p} modes. However, in the case of non-symmetric TE_{mn} modes radiating from oversized open-ended circular waveguides also the coupling to reflected TM_{mp} modes with the same direction of polarization is existent.

Acknowledgment

The authors would like to acknowledge the staff members in the workshop of the IPF Stuttgart for their enthusiasm, effort, and skill in the precise manufacture of the nonlinear TE_{01}-mode up-taper, the various mode converters, and the wavenumber spectrometer. The authors also wish to express their deep gratitude to M. Huber, C. Kastner, and B.-J. Bobach for carefully preparing this manuscript.

References

[1] M. Thumm, "High power gyro-devices for plasma heating and other applications," *Int. J. Infrared Millim. Waves*, vol. 26, pp. 483–503, 2005.

[2] H. G. Unger, "Circular waveguide taper of improved design," *Bell Syst. Tech. J.*, vol. 37, pp. 899–912, 1958.

[3] A. Wien and M. Thumm, "Numerical analysis of backscattering from a helically cut quasi-optical antenna," in *19th Int. Conf. Infrared Millim. Waves Conf. Dig.*, Sendai, Japan, 1994, pp. 337–338, Paper AP941228.

[4] D. Wagner, M. Thumm, W. Kasparek, G. A. Müller, and O. Braz, "Prediction of TE-, TM-, and hybrid-mode transmission losses in gaps of oversized waveguides using a scattering matrix code," *Int. J. Infrared Millim. Waves*, vol. 17, pp. 1071–1081, 1996.

[5] *"User and Reference Manual for the 3D EM Time Domain Simulator Empire XCcel"* ver. 6.0, IMST GmbH, 2012 [Online]. Available: http://www.empire.de/

[6] H. Y. Yee and L. B. Felsen, "Ray-optical analysis of electromagnetic scattering in waveguides," *IEEE Trans. Microw. Theory Tech.*, vol. MTT–17, no. 9, pp. 671–683, 1969.

[7] J. B. Keller, "Geometrical theory of diffraction," *J. Opt. Soc. Amer.*, vol. 52, pp. 116–130, 1962.

[8] L. A. Weinstein, *Theory of Diffraction and the Factorization Method*. Boulder, CO, USA: The Golem Press, 1969.

[9] A. Wien and M. Thumm, "Numerical analysis of quasi-optical mode converter, Part 1: Backscattering analysis of shaped-end radiators," *Int. J. Electron.*, vol. 86, pp. 739–745, 1999.

[10] A. Michaeli, "Equivalent edge currents for arbitrary aspects of observation," *IEEE Trans. Antennas Propag.*, vol. 32, no. 3, pp. 252–258, 1984.

[11] M. Thumm, "High-power millimetre-wave mode converters in overmoded circular waveguides using periodic wall perturbations," *Int. J. Electron.*, vol. 57, pp. 1225–1246, 1984.

[12] H. Kumric, M. Thumm, and R. Wilhelm, "Optimization of mode converters for generating the fundamental TE_{01} mode from TE_{06} Gyrotron output at 140 GHz," *Int. J. Electron.*, vol. 64, pp. 77–94, 1988.

[13] W. Kasparek and G. Müller, "The wavenumber spectrometer," *Int. J. Electron.*, vol. 64, pp. 5–20, 1988.

[14] G. Piefke, "Reflection at incidence of an H_{mn}-wave at junction of circular waveguide and circular horn," in *Symposium on Electromagnetic Theory and Antennas*. Copenhagen, Denmark: Pergamon Press, 1962, pp. 209–234.

[15] T. Itoh and R. Mittra, "A new method of solution for radiation from a flanged waveguide," *Proc. Inst. Electr. Eng.*, vol. 59, pp. 1131–1133, 1971.

[16] F. Reisdorf and W. Schmnke, "Applications of a "Zwischenmedium" to the radiation from a flanged waveguide," *Proc. Inst. Electr. Eng.*, vol. 120, pp. 739–740, 1973.